Energy 77 (2014) 562–569

Contents lists available at ScienceDirect

Energy

journal homepage: www.elsevier.com/locate/energy

Modeling and performance analysis of a two-stage thermoelectric energy harvesting system from blast furnace slag water waste heat

Bing Xiong [a, b, c], Lingen Chen [a, b, c, *], Fankai Meng [a, b, c], Fengrui Sun [a, b, c]

[a] Institute of Thermal Science and Power Engineering, Naval University of Engineering, Wuhan 430033, China
[b] Military Key Laboratory for Naval Ship Power Engineering, Naval University of Engineering, Wuhan 430033, China
[c] College of Power Engineering, Naval University of Engineering, Wuhan 430033, China

ARTICLE INFO

Article history:
Received 23 April 2014
Received in revised form
23 August 2014
Accepted 13 September 2014
Available online 7 October 2014

Keywords:
Two-stage thermoelectric generator
Variable-temperature heat reservoirs
Blast furnace slag water
Waste heat recovery

ABSTRACT

A physical and numerical model of two-stage thermoelectric energy harvesting system driven by blast furnace slag water waste heat is established. The performance of the system with counter-flow type heat exchangers is investigated by numerical simulation. In the case of the temperatures of heat reservoirs change over flow passage, the effects of inlet temperature of flushing slag water, convective heat transfer coefficient and flow passage length on the power output, efficiency, maximum power output and maximum efficiency as well as optimal resistance ratio of the system are analyzed. Moreover, the electrical current range corresponding to the maximum power output and maximum efficiency is obtained. Simulation results show that the maximum power output of 0.44 kW and maximum efficiency of 2.66% are available with inlet temperature of blast furnace slag water at 100 °C if load resistance is matched. The optimal resistance ratio corresponding to the maximum power output is about 1.13.

1. Introduction

Thermoelectric generation is classified as direct power conversion [1–5]. It has lots of features and advantages compared with traditional generators, for example, the absence of moving components results in an increase of reliability, and reduction of extra maintenance; the modularity can provide a wide-scale application without significant losses in performance. Besides, these devices produce no noise and waste in the conversion process. Therefore, thermoelectric generator has been regarded as a useful and attractive device for direct energy conversion [6–10] and potential application in waste heat recovery [11–14].

As energy shortage and environmental deterioration are growing, energy saving and emission reduction have become global obligation and responsibility [15–19]. Yu and Zhao [15] employed hot and cold water as heat reservoirs and analyzed the performance of thermoelectric generator with the parallel-plate heat exchanger. Meng et al. [16] established a numerical model of commercial thermoelectric generator with finned heat exchangers taking into account inner and external multi-irreversibilities. Gou et al. [17] established a dynamic model for waste heat recovery in thermoelectric generator to assess the effects of heat reservoirs on the dynamic characteristics. Kazuaki et al. [18] analyzed energy economy for a combined thermoelectric generator on top of a steam turbine cycle, and demonstrated the advantage of adding a thermoelectric on top of a steam turbine cycle. Stevens [19] established an energy harvesting device that produces milliwatt-scale power uses a thermoelectric generator operating between the air and ground temperatures.

Since the single stage thermoelectric generator cannot operate in the case of large temperature range [20–25], and due to the performance limits of thermoelectric materials and requirements of adapting different heat reservoir conditions, some authors have investigated the performance of thermoelectric generator composed of two stages and more [26–32].

In the process of promoting the transformation of materials in the iron and steel industry, rich and variety of waste heat is generated. Taking advantage of these waste heats can effectively reduce energy consumption [33–35]. Chen et al. [36] provided an overview of residual heat recovery in iron and steel enterprises in China based on single stage and multi-element thermoelectric generation, and the calculations showed that electricity power of 21 kWh, 43 kWh and 60 kWh can be recovered from 1 GJ waste heat with temperature difference of 100 °C, 200 °C and 300 °C, respectively. Meng et al. [37] established a model of single stage

* Corresponding author. College of Power Engineering, Naval University of Engineering, Wuhan 430033, China. Tel.: +86 27 83615046; fax: +86 27 83638709.
E-mail addresses: lgchenna@yahoo.com, lingenchen@hotmail.com (L. Chen).

http://dx.doi.org/10.1016/j.energy.2014.09.037
0360-5442/

Nomenclature

A	area (m^2)
B	flow channel width (m)
c	specific heat capacity at constant pressure (J kg^{-1} K^{-1})
G	mass flow rate (kg s^{-1})
H	flow channel height (m)
h	convective heat transfer coefficient (W m^{-2} K^{-1})
I	electrical current (A)
K	thermal conductance (W K^{-1})
L	length (m)
P	power output (W)
Q	heat flow rate (W)
R	electrical resistance (Ω)
r	load resistance ratio
T	thermodynamic temperature (K)
t	Celsius temperature (°C)

Greek symbol

α	Seebeck coefficient (V K^{-1})
σ	electrical conductivity (Ω^{-1} m^{-1})
λ	thermal conductivity (W m^{-1} K^{-1})
θ	fill factor
η	conversion efficiency

Subscripts

c	cold junction
f	flow passage
g	air gap
h	hot junction
L	load
m	intermediate junction
1	heat source
2	heat sink

and multi-element thermoelectric generator driven by blast furnace slag flushing water sensible heat with parallel-flow type heat exchangers, and analyzed the power and efficiency performance, as well as the recovery period of the equipment cost.

On the basis of research achievements mentioned above, this paper will establish a physical and numerical model of two stage thermoelectric energy harvesting system driven by blast furnace slag water waste heat, and analyze the effects of key parameters on the power output, efficiency, optimal electrical current as well as optimal resistance ratio of the system.

2. Harvesting system setup and model

A schematic diagram of the harvesting system driven by blast furnace slag water waste heat is shown in Fig. 1. The system is consisted of two parts. The first part contains two heat exchangers between heat reservoir and two-stage thermoelectric generator module. As is well known, the performance of counter-flow heat exchanger is better than that of parallel-flow one, this paper aims at discussing the system's performance with counter-flow type heat exchangers between blast furnace slag water and cooling water. The second part is the two-stage thermoelectric generator. The waste slag washing water flows through the hot-side heat-exchanger channels and heats the upper surface of thermoelectric module. The cooling water driven by a pump flows through the cold-side heat-exchanger channels and absorbs heat from the lower surface of thermoelectric modules.

The generator consisted of a top stage and a bottom stage with the same pairs of thermoelectric elements. Each element is composed of p-type and n-type semiconductor legs. The thermoelectric power-generation element is assumed to be insulted, both electrically and thermally, from its surroundings, except at the junction-reservoir contacts and the junction between the two stages. The structure parameters of two heat-exchangers and the geometric dimensions of each element of the two-stage modules are assumed to be the same.

The thermodynamic model of two-stage thermoelectric generator system driven by blast furnace slag waste heat is shown in Fig. 2. The temperatures of slag washing water and cooling water are $T_1(x)$ and $T_2(x)$, respectively. The temperatures of the hot-junction and cold-junction are $T_h(x)$ and $T_c(x)$, respectively. The top stage and bottom stage of the thermoelectric generator are assumed to be well contacted, so the thermal contact resistance between the two modules is neglected. The temperature of the cold-side junction of top stage and the temperature of the hot-side junction of bottom stage are assumed to be the same, i.e. $T_m(x)$.

Since the thermoelectric thermocouples are not closely packed for insulation, there exists an air gap between the thermocouples. Thus heat flow from the heat reservoir directly flows through the air gap rather than through the thermocouples, and the heat flow is

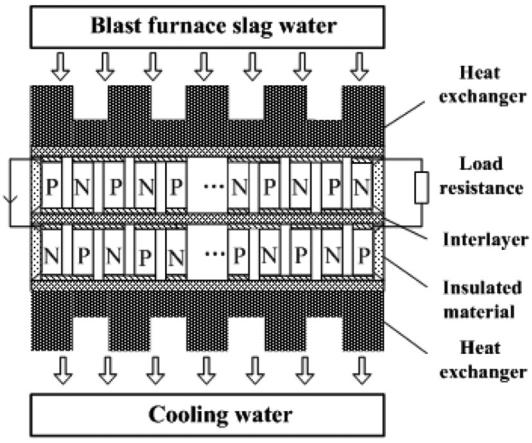

Fig. 1. Schematic diagram of two-stage thermoelectric generator system driven by blast furnace slag water waste heat.

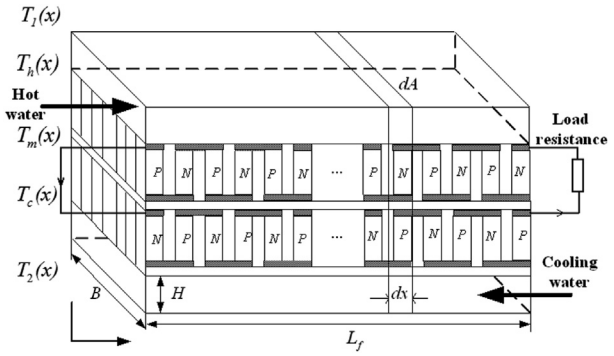

Fig. 2. Thermodynamic model of two-stage thermoelectric generator system driven by waste heat.

expressed by Q_g. Taking into account the heat flow through the air gap between the thermocouples, the fill factor θ ($0 < \theta \leq 1$) [22] is introduced to express the proportion of the thermoelectric elements area on the modules:

$$\theta = 2AN/A_{cp} \tag{1}$$

where A, N and A_{cp} are, respectively, the cross-sectional area of thermo-elements, the number of thermocouples in a module, and the cross-sectional area of a module. The heat flow rate of the air gap leakage of top stage generator and bottom stage generator is Q_{g1} and Q_{g2}, respectively.

For the top stage generator, the heat flow rate absorbed from the heat source is Q_1. For the bottom stage generator, the heat flow rate dissipated to the heat sink is Q_2. Moreover, the rates of heat absorption and dissipation at hot junction of top stage generator are Q_{h1} and Q_{c1}, respectively. The rates of heat absorption and dissipation at cold junction of bottom stage generator are Q_{h2} and Q_{c2}, respectively. The two stage thermoelectric generator is connected electrically in series along the directions of fluid path, but in parallel for the directions perpendicular to fluid path. The power output of the system is P. The electrical resistance of the external load and single element are R_L and R, respectively. The electrical current generating through the system at steady condition is I. The heat conductances of hot and cold side heat-exchanger are K_1 and K_2, and both of them are calculated from four thermal resistances: heat exchanger separator resistances δ_{ex}/λ_{ex}, ceramic substrate resistances δ_{cp}/λ_{cp} and convective heat transfer resistances $1/h_{cv}$ as well as heat conduction grease contact resistances δ_c/λ_c. That is:

$$K_1 = \frac{1}{\delta_{ex}/\lambda_{ex} + \delta_{cp}/\lambda_{cp} + 1/h_{cv} + \delta_c/\lambda_c}, \quad K_2 = K_1 \tag{2}$$

A control volume shown in Fig. 2 is formulated for a set of elements, which includes flow passages on both sides of the thermoelectric generator. Thus, the governing equations of the control volume for the top stage generator, respectively, are

$$\mathrm{d}Q_1 = -G_1 c_{p1}\,\mathrm{d}T_1(x) \tag{3}$$

$$\mathrm{d}Q_1 = K_1[T_1(x) - T_h(x)]B\,\mathrm{d}x \tag{4}$$

$$\mathrm{d}Q_{h1} = \left[\alpha T_h(x)I + K(T_h(x) - T_m(x)) - \frac{I^2R}{2}\right]\frac{\theta B\,\mathrm{d}x}{2A} \tag{5}$$

$$\mathrm{d}Q_{c1} = \left[\alpha T_m(x)I + K(T_h(x) - T_m(x)) + \frac{I^2R}{2}\right]\frac{\theta B\,\mathrm{d}x}{2A} \tag{6}$$

where G_1, c_{p1}, B, α and K are, respectively, the rate of blast furnace slag water flow, specific heat at constant pressure of blast furnace slag water, width of fluid passage, Seebeck coefficient, thermal conductance.

Making the same analyses for bottom stage generator, one has:

$$\mathrm{d}Q_2 = -G_2 c_{p2}\,\mathrm{d}T_2(x) \tag{7}$$

$$\mathrm{d}Q_2 = K_2[T_c(x) - T_2(x)]B\,\mathrm{d}x \tag{8}$$

$$\mathrm{d}Q_{h2} = \left[\alpha T_m(x)I + K(T_m(x) - T_c(x)) - \frac{I^2R}{2}\right]\frac{\theta B\,\mathrm{d}x}{2A} \tag{9}$$

$$\mathrm{d}Q_{c2} = \left[\alpha T_c(x)I + K(T_m(x) - T_c(x)) + \frac{I^2R}{2}\right]\frac{\theta B\,\mathrm{d}x}{2A} \tag{10}$$

where G_2, c_{p2} are, respectively, the rate of cooling water flow, specific heat at constant pressure of cooling water.

The heat flow rates of the air gap leakage of top stage generator and bottom stage generator are, respectively:

$$\mathrm{d}Q_{g1} = K_{g1}(T_h(x) - T_m(x))(1-\theta)B\,\mathrm{d}x \tag{11}$$

$$\mathrm{d}Q_{g2} = K_{g2}(T_m(x) - T_c(x))(1-\theta)B\,\mathrm{d}x \tag{12}$$

where K_{g1} and K_{g2} are, respectively, the heat conductance of the air gap leakage of top stage generator and bottom stage generator. $K_{g1} = K_{g2} = \lambda_{air}/L$, where λ_{air} is the thermal conductivity of air, and L is the length of a single element.

Based on the energy balance, one has:

$$Q_1 = Q_{h1} + Q_{g1} \tag{13}$$

$$Q_m = Q_{c1} + Q_{g1} = Q_{h2} + Q_{g2} \tag{14}$$

$$Q_2 = Q_{c2} + Q_{g2} \tag{15}$$

Substituting Eqs. (3)–(12) into Eqs. (13)–(15) yields the differential equations about $T_1(x)$, $T_h(x)$, $T_m(x)$, $T_c(x)$ and $T_2(x)$ as

$$T_1'(x) = \frac{K_1[T_1(x) - T_h(x)]B}{-G_1 c_{p1}} \tag{16}$$

$$K_1(T_1(x) - T_h(x)) = \left[\alpha T_h(x)I + K(T_h(x) - T_m(x)) - \frac{I^2R}{2}\right]\frac{\theta}{2A} + K_{g1}(T_h(x) - T_m(x))(1-\theta) \tag{17}$$

$$\left[K_{g1}(T_h(x) - T_m(x)) - K_{g2}(T_m(x) - T_c(x))\right](1-\theta) = \left[K(2T_m(x) - T_c(x) - T_h(x)) - I^2R\right]\frac{\theta}{2A} \tag{18}$$

$$K_2(T_c(x) - T_2(x)) = \left[\alpha T_c(x)I + K(T_m(x) - T_c(x)) + \frac{I^2R}{2}\right]\frac{\theta}{2A} + K_{g2}(T_m(x) - T_c(x))(1-\theta) \tag{19}$$

$$T_2'(x) = \frac{K_2[T_c(x) - T_2(x)]B}{-G_2 c_{p2}} \tag{20}$$

The boundary conditions of temperatures of fluids for counter-flow type heat exchangers are:

$$T_1(0) = T_{10} \tag{21}$$

$$T_2\left(L_f\right) = T_{20} \tag{22}$$

where L_f is the length of the flow passages for two heat-exchangers.

The power output P of the system is the difference between the absorbed and dissipated heat flow rate, and the thermal efficiency of the system is $\eta = P/Q_1$. Then, one has

$$P = G_1 c_{p1}\left[T_1(0) - T_1\left(L_f\right)\right] - G_2 c_{p2}\left[T_2(0) - T_2\left(L_f\right)\right] \tag{23}$$

$$\eta = 1 - \frac{G_2 c_{p2}\left[T_2(0) - T_2\left(L_f\right)\right]}{G_1 c_{p1}\left[T_1(0) - T_1\left(L_f\right)\right]} \tag{24}$$

The differential equations (16)–(20) belong to the two-point boundary value problems, which cannot be directly solved with ordinary methods. In this paper, trial method is used to translate the boundary value problem into initial value problem that can be solved by numerical method. The calculation flow chart of differential equations is shown in Fig. 3. The initial $T_2(0)$ is input for calculating the differential equations, and the accurate $T_2(0)$ can be determined through the judge and loop statements. Thus, the temperatures that vary with the flow passage, i.e. $T_1(x)$, $T_h(x)$, $T_m(x)$, $T_c(x)$ and $T_2(x)$ can be calculated, the analytical formula describing the power output and efficiency versus the key parameters are derived.

3. Numerical examples and analyses

The effects of some key parameters on the system's performance are investigated by numerical simulation. Since the inlet temperature of blast furnace slag water at constant pressure is less than 100 °C and the inlet temperature of cooling water is set as 20 °C, the effect of temperature on the physical properties of the thermoelectric materials is ignored. The physical properties of the thermoelectric materials at mean temperature of 50 °C are set as follows [38]: $\alpha = 2.07 \times 10^{-4}$ V K^{-1}, $\lambda = 1.53$ W m^{-1} K^{-1}, and $\sigma = 8.70 \times 10^4$ m Ω^{-1}. The length and cross-sectional area of a thermoelectric semiconductor leg are $L = 2.0 \times 10^{-3}$ m and $A = 1.2 \times 1.2 \times 10^{-6}$ m^2, respectively, the fill factor can be calculated as $\theta = 0.5$. The plate heat exchangers are made of aluminum. The thickness of heat exchangers is $\delta_{ex} = 2.0 \times 10^{-3}$ m, the width of the flow channel is $B = 0.1$ m, and the height of the flow channel is $H = 6.0 \times 10^{-3}$ m. The specific heats of blast furnace slag water and cooling water at constant pressure are $c_{p1} = 4.2 \times 10^3$ J kg^{-1} K^{-1} and $c_{p2} = 4.18 \times 10^3$ J kg^{-1} K^{-1}, respectively. The mass flow rates and flow velocity of water are set as $G_1 = G_2 = 0.6$ kg s^{-1} and $v_1 = v_2 = 1.0$ m/s, respectively. Besides, since the estimated pumping power (several watts) is quite small compared with the power output of the systems, the effect of pump power and its energy consumption is not taken into account.

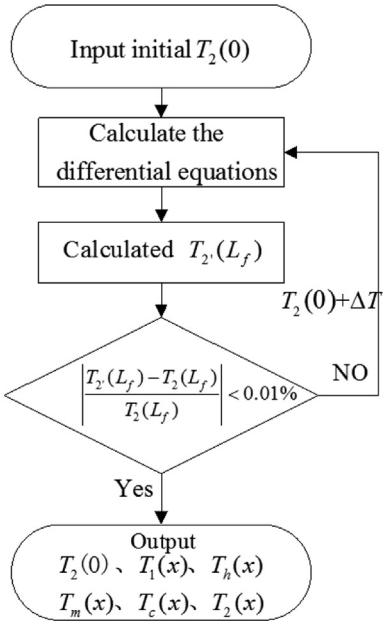

Fig. 3. Calculation flow chart of differential equations.

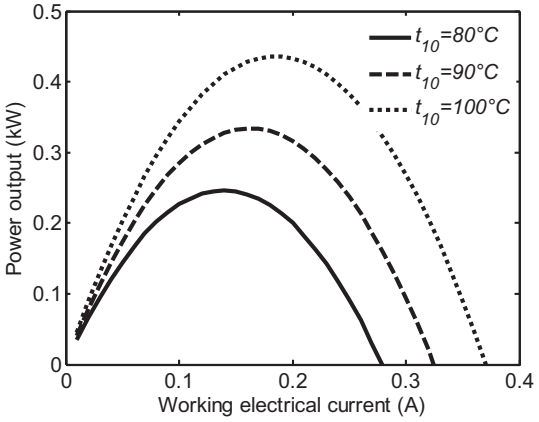

Fig. 4. Effect of inlet temperature of flushing slag water on power versus electrical current.

3.1. The effects of inlet temperature of blast furnace slag water

Figs. 4 and 5 show the effects of blast furnace slag water inlet temperature on power output and efficiency versus working electrical current, respectively. Since the two heat reservoirs are driven by water pump and defined as forced convective heat transfer, the convective heat transfer coefficient of water is calculated as $h_{cv} = 3000$ W m^{-2} K^{-1} based on the heat exchanger geometry. It can be seen that the power output and efficiency versus working electrical current characteristic behaves a parabola-like for fixed inlet temperature of blast furnace slag water. There are two optimal working electrical currents I_P and I_η corresponding to the maximum power output and maximum efficiency, respectively. Both the power output and efficiency increase with the increase of inlet temperature of blast furnace slag water. The maximum power output of 0.44 kW and maximum efficiency of 2.66% are available for inlet temperature of blast furnace slag water at 100 °C if load resistance is matched.

Fig. 6 shows the variation of maximum power output and maximum efficiency with the inlet temperature of blast furnace slag water. It can be seen that both the maximum power output and maximum efficiency increase with the inlet temperature of blast furnace slag water. Moreover, the maximum efficiency is a linear increasing function of the inlet temperature of blast furnace slag water. However, the maximum power output is a nonlinearly increasing function of inlet temperature of blast furnace slag water and the growth rate is larger and larger. Fig. 7 shows the variation of

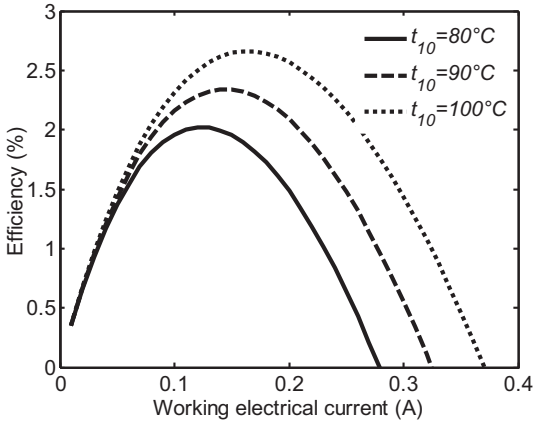

Fig. 5. Effect of inlet temperature of flushing slag water on efficiency versus electrical current.

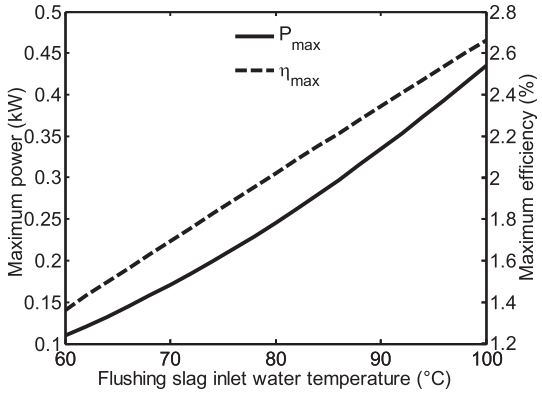

Fig. 6. The maximum power and maximum efficiency versus inlet temperature of flushing slag water.

the optimal working electrical currents with the inlet temperature of blast furnace slag water. It can be seen that both I_P and I_η are linear increasing functions of the inlet temperature of blast furnace slag water, and the optimal working electrical current (I_P) corresponding to the maximum power output is larger than that (I_η) corresponding to the maximum efficiency for fixed inlet temperatures. The intermediate range between two lines is the optimal working region of electrical current. Therefore, an appropriate working electrical current should be determined in order to meet different needs in practical applications.

The inlet temperature of blast furnace slag water as industrial circulating water at constant pressure is less than 100 °C. However, it is suggested that hot water/glycol mixture fluids could be an appropriate choice for the temperature over 100 °C in practical application [15]. Calculation results show that the maximum power output and maximum efficiency of the system can, respectively, reach to 1.14 kW and 4.20% for inlet temperature of blast furnace slag water at 150 °C, they are respectively 162% and 57.8% improvements than those of the system with inlet temperature of blast furnace slag water at 100 °C. To sum up, the increase of inlet temperature of blast furnace slag water can significantly improve the performance of the system.

3.2. The effects of convective heat transfer coefficient

Figs. 8 and 9 show the effects of convective heat transfer coefficient on power output and efficiency versus working electrical current, respectively. Fig. 10 shows the variation of maximum power output and maximum efficiency versus the convective heat

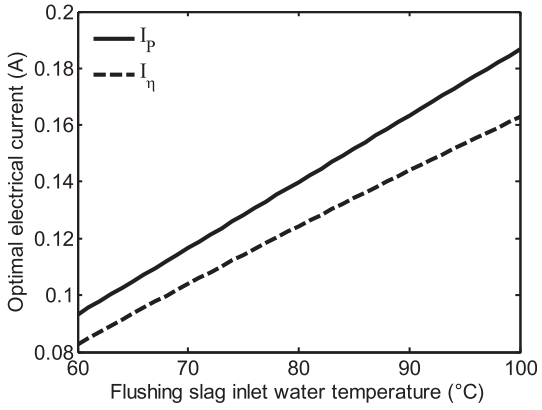

Fig. 7. Optimal electrical currents versus inlet temperature of flushing slag water.

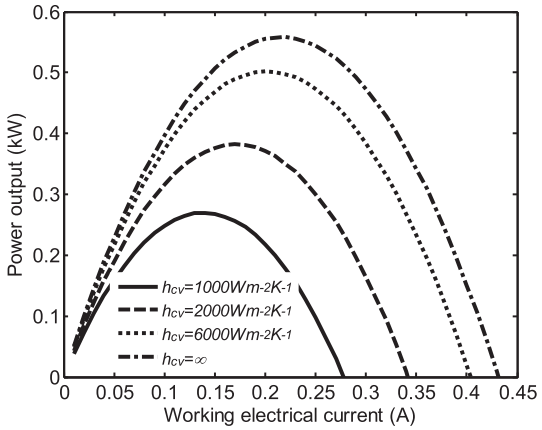

Fig. 8. Effect of convective heat transfer coefficient on power versus electrical current.

transfer coefficient. In the calculations, $L_f = 10$ m and $t_{10} = 100$ °C are set. It can be seen that both the power output and efficiency increase with the increase of the convective heat transfer coefficient. However, the growth rate is smaller and smaller as the increase of the convective heat transfer coefficient. The convective heat transfer coefficient of water is about 3000–5000 W m^{-2} K^{-1}, the maximum power output of 0.49 kW and maximum efficiency of 2.81% are available for inlet temperature of blast furnace slag water at 100 °C. When the external heat resistance losses between the thermoelectric generator and the external reservoir are ignored, i.e. $h_{cv} \to \infty$, the maximum power output and maximum efficiency are 0.58 kW and 3.06%, respectively.

Figs. 11 and 12 show the optimal working electrical current and optimal resistance ratio versus convective heat transfer coefficient, respectively. It can be seen that the optimal working electrical current I_{opt} increases, while the optimal resistance ratio r_{opt} decreases with the increase of convective heat transfer coefficient at the beginning. However, both I_{opt} and r_{opt} tend to be stable as the convective heat transfer coefficient increases. Moreover, $I_P > I_\eta$ and $r_\eta > r_P$ are guaranteed for a fixed convective heat transfer coefficient. The optimal resistance ratio corresponding to the maximum power output is about 1.13 and that corresponding to the maximum efficiency is about 1.42 with the convective heat transfer coefficient of 3000 W m^{-2} K^{-1}.

It should be pointed out that most of previous researches about the thermoelectric generator were performed by using non-equilibrium thermodynamics without considering the external

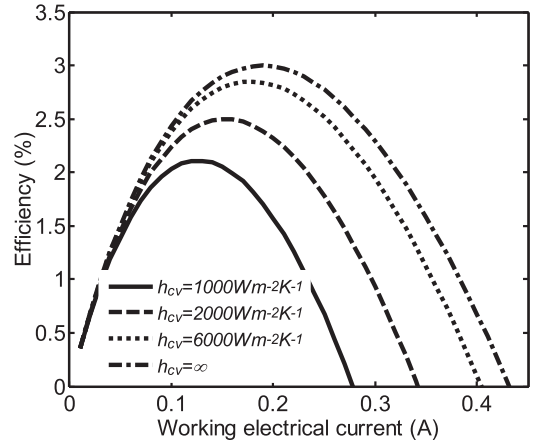

Fig. 9. Effect of convective heat transfer coefficient on efficiency versus electrical current.

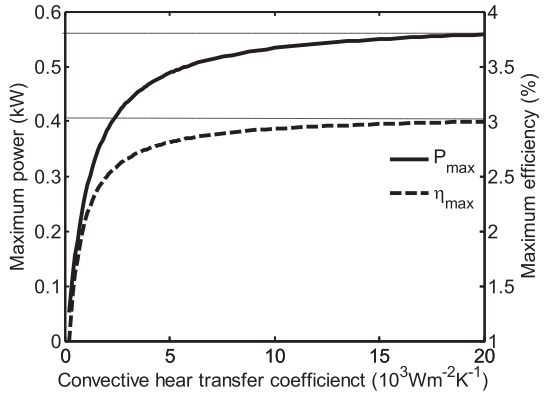

Fig. 10. The maximum power and maximum efficiency versus convective heat transfer coefficient.

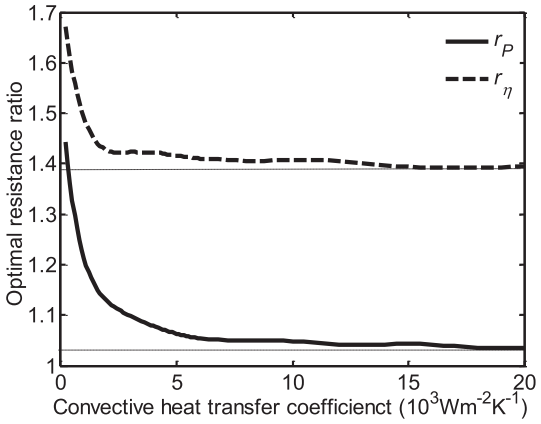

Fig. 12. Optimal resistance ratio versus convective heat transfer coefficient.

heat resistance losses and were based on the infinite thermal capacity, i.e. constant temperature heat reservoirs. In this case, the load resistance is selected to equal to the effective internal resistance of the thermoelectric generator so that the maximum power output of the system could be achieved [15,37], i.e. $r_P = 1$. However, the heat reservoirs in practical application are always finite-capacity and variable-temperature. Thus, the temperatures of the modules vary with some key factors, such as working electrical current and convective heat transfer coefficient. Calculation results show that the optimal resistance ratio corresponding to the maximum power output is $r_P > 1$. Therefore, the external heat resistance losses cannot be ignored.

3.3. The effects of flow passage length

Fig. 13 shows the effects of flow passage length on the maximum power output and maximum efficiency, respectively. Fig. 14 is employed to show how the power per area changes with the flow passage. In the calculations, $t_{10} = 100\ ^\circ\mathrm{C}$ and $h_{cv} = 3000\ \mathrm{W\ m^{-2}\ K^{-1}}$ are set. It can be seen that the maximum power output increases with the increase of flow passage length, while both the maximum efficiency and maximum power-per-area are linear decreasing functions of the flow passage length. It results from the decrease of temperature of blast furnace slag water along the flow passage and then the temperature difference through the modules.

Fig. 15 shows the effect of flow passage length on the optimal working electrical current. It can be seen that the two optimal working electrical currents corresponding to the maximum power output and the maximum efficiency are linear decreasing functions of the flow passage length. Moreover, $I_P > I_\eta$ is guaranteed for fixed flow passage length. The intermediate range between two lines is the optimal working region of electrical current.

4. Conclusion

This paper establishes a model of two-stage thermoelectric energy harvesting system. The performance of the two-stage thermoelectric generator system driven by blast furnace slag water waste heat is analyzed. The major results are as follows:

(1) The inlet temperature of flushing slag water is an important parameter which affects the performance of the two-stage thermoelectric generator system significantly. Both the maximum efficiency and the optimal working electrical current are linear increasing functions of the flushing slag water inlet temperature, while the maximum power output is nonlinear.
(2) The optimal resistance ratio corresponding to the maximum power output is about 1.13 and the optimal resistance ratio corresponding to the maximum efficiency is 1.42 in the case of external heat resistance losses between the device and heat reservoirs are taking into account.
(3) Both the maximum efficiency and the growth rate of the maximum power output decrease with increase of flow passage while the maximum power output increases. Moreover, the two optimal working electrical currents decrease.

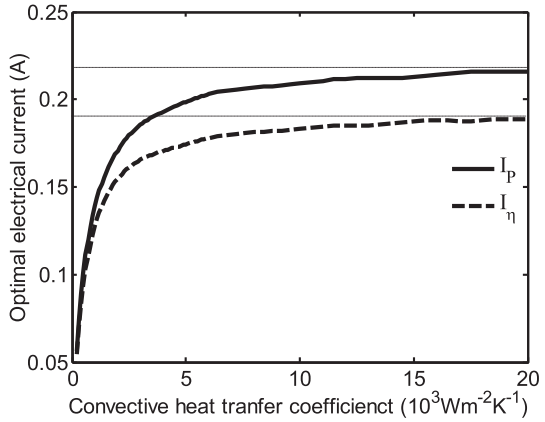

Fig. 11. Optimal electrical currents versus convective heat transfer coefficient.

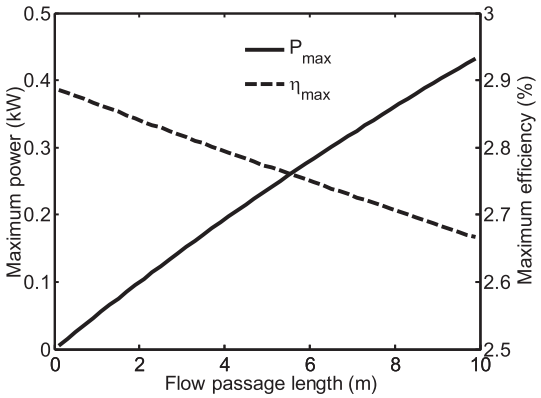

Fig. 13. The maximum power and maximum efficiency versus flow passage length.

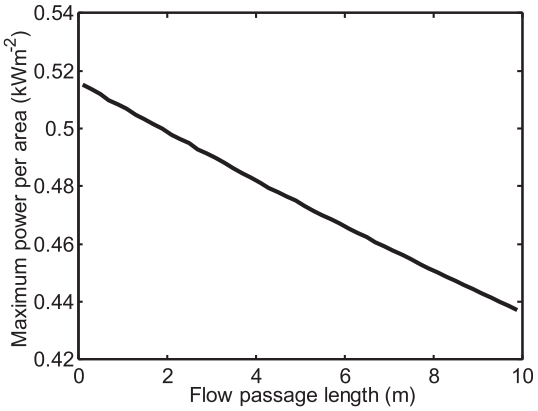

Fig. 14. The maximum power per unit heat transfer surface area versus flow passage length.

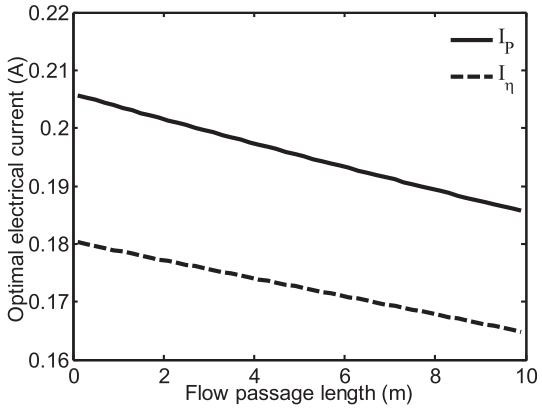

Fig. 15. Optimal electrical currents versus flow passage length.

(4) The maximum power output of 0.44 kW and maximum efficiency of 2.66% are available with the inlet temperature of blast furnace slag water at 100 °C if load resistance is matched. Moreover, the maximum power output and maximum efficiency can, respectively, reach to 1.14 kW and 4.20% if the inlet temperature of flushing slag water increases to 150 °C.

The physical and numerical model is a general model that can be applied to different forms of heat reservoir, i.e. water or gas, moreover, the energy harvesting system can adapt to large temperature range of waste heat due to the two-stage configuration. Further work is to setup an equipment device and obtain experiment data. The results obtained herein may provide some guidelines for the design and application of practical two-stage thermoelectric generator system in the iron and steel industry.

Acknowledgments

This paper is supported by the National Basic Research Program of China (No. 2012CB720405) and the National Natural Science Foundation of China (No. 11305266). The authors wish to thank the reviewers for their careful, unbiased and constructive suggestions, which led to this revised manuscript.

References

[1] Ioffe AF. Semiconductor thermoelements and thermoelectric cooling. London: Infosearch; 1957.
[2] Okhotin AS, Pushkarsky AS. New criterion of thermoelectric material efficiency. Dokl Akad NAUK SSSR 1972;203(2):336.
[3] Rowe DM. CRC handbook of thermoelectrics. 1st ed. Boca Raton: CRC Press; 1995.
[4] Goupil C, Seifert W, Zabrocki K, Muller E, Snyder GJ. Thermodynamics of thermoelectric phenomena and applications. Entropy 2011;13(8):1481–517.
[5] Date Ashwin, Date Abhijit, Dixon Chris, Akbarzadeh Aliakbar. Progress of thermoelectric power generation systems: prospect for small to medium scale power generation. Renew Sustain Energy Rev 2014;33:371–81.
[6] Chen M, Rosendahl L, Bach I, Condra T, Pedersen J. Irreversible transfer processes of thermoelectric generators. Am J Phys 2007;75(9):815–20.
[7] Astrain D, Vián JG, Martínez A, Rodríguez A. Study of the influence of heat exchangers' thermal resistances on a thermoelectric generation system. Energy 2010;35(2):602–10.
[8] Rezania A, Rosendahl LA. Thermal effect of a thermoelectric generator on parallel microchannel heat sink. Energy 2012;37(1):221–7.
[9] Sahin AZ, Yilbas BS. Thermodynamic irreversibility and performance characteristics of thermoelectric power generator. Energy 2013;55:899–904.
[10] Montecucco A, Knox AR. Accurate simulation of thermoelectric power generating systems. Appl Energy 2014;118:166–72.
[11] Ismail BI, Ahmed WH. Thermoelectric power generation using waste-heat energy as an alternative green technology. Recent Pat Electr Eng 2009;2(1):27–39.
[12] Gou X, Xiao H, Yang S. Modeling, experimental study and optimization on low-temperature waste heat thermoelectric generator system. Appl Energy 2010;87(10):3131–6.
[13] Karri MA, Thacher EF, Helenbrook BT. Exhaust energy conversion by thermoelectric generator: two case studies. Energy Convers Manag 2011;52(3):1596–611.
[14] Jang JY, Tsai YC. Optimization of thermoelectric generator module spacing and spreader thickness used in a waste heat recovery system. Appl Therm Eng 2013;51(1–2):677–89.
[15] Yu J, Zhao H. A numerical model for thermoelectric generator with the parallel-plate heat exchanger. J Power Sources 2007;172(1):428–34.
[16] Meng F, Chen L, Sun F. A numerical model and comparative investigation of a thermoelectric generator with multi-irreversibilities. Energy 2011;26(5):3513–22.
[17] Gou X, Yang S, Xiao H, Ou Q. A dynamic model for thermoelectric generator applied in waste heat recovery. Energy 2013;52:201–9.
[18] Kazuaki Y, Yee RK, Ali S. Optimization of thermoelectric topping combined steam turbine cycles for energy economy. Appl Energy 2013;109:1–9.
[19] Stevens JW. Performance factors for ground-air thermoelectric power generators. Energy Convers Manag 2013;68:114–23.
[20] Ivanjuk AP, Okhotin AS, Pushkarsky AS. On some new criteria of efficiency of thermoelectric materials. Energy Convers 1977;17(1):19–21.
[21] Sun F, Chen W, Chen L. The finite time thermodynamics optimization criterion of thermoelectric generator. J Eng Thermophys 1993;14(1):13–5 [in Chinese].
[22] Rowe DM, Min G. Evaluation of thermoelectric modules for power generation. J Power Sources 1998;73(2):193–8.
[23] Chen L, Sun F, Wu C. Heat transfer surface area optimization for a thermoelectric generator. Int J Ambient Energy 2007;28(3):135–42.
[24] Lesage FJ, Potvin N. Experimental analysis of peak power output of a thermoelectric liquid-to-liquid generator under an increasing electrical load resistance. Energy Convers Manag 2013;66:98–105.
[25] Chen L, Meng F, Sun F. Internal and external simultaneous optimization of an irreversible thermoelectric generator for maximum power output. Int J Low-Carbon Technol 2013;8(3):188–96.
[26] Chen L, Li J, Sun F, Wu C. Performance optimization of a two-stage semiconductor thermoelectric generator. Appl Energy 2005;82(4):300–12.
[27] Li KZ, Liang RS, Wei ZJ. Analysis of performance and optimum configuration of two-stage semiconductor thermoelectric module. Chin Phys B 2008;17(4):1349–56.
[28] Ramírez-López C, Olivares-Robles MA. Optimization of two-stage Peltier module with the method of Yamanashi and exergy analysis of the system. In: Paper presented at 5th international workshop on non-equilibrium thermodynamics IWNET 2009, at Eternal Spring City of Cuernavaca, Mexico, 24–28 August 2009; 2009.
[29] Bélanger S, Gosselin L. Thermoelectric generator sandwiched in a crossflow heat exchanger with optimal connectivity between modules. Energy Convers Manag 2011;52(8–9):2911–8.
[30] Olivares-Robles NMA, Vazquez F, Ramirez-Lopez C. Optimization of two-stage Peltier modules: structure and exergy efficiency. Entropy 2012;14(8):1539–52.
[31] Wang CC, Hung CI, Chen WH. Design of heat sink for improving the performance of thermoelectric generator using two-stage optimization. Energy 2012;39:236–45.
[32] Reddy BVK, Barry M, Li J, Chyu MK. Thermoelectric-hydraulic performance of a multistage integrated thermoelectric power generator. Energy Convers Manag 2014;77:458–68.
[33] Chen WH, Liao CY, Hung CI, Huang WL. Experimental study on thermoelectric modules for power generation at various operating conditions. Energy 2012;45:874–81.
[34] Zhang H, Dong L, Li H. Investigation of the residual heat recovery and carbon emission mitigation potential in a Chinese steelmaking plant: a hybrid material/energy flow analysis case study. Sustain Energy Technol Assess 2013;2:67–80.

[35] Zheng XF, Liu CX, Yan YY, Wan Q. A review of thermoelectrics research – recent developments and potentials for sustainable and renewable energy applications. Renew Sustain Energy Rev 2014;32:486–503.
[36] Chen L, Meng F, Sun F. Analysis of energy-saving potential based on thermoelectric generation for iron and steel industry waste heat recovery. Res Iron Steel 2013;41(6):41–3 [in Chinese].
[37] Meng F, Chen L, Sun F, Yang B. Thermoelectric power generation driven by blast furnace slag flushing water. Energy 2014;66:965–72.
[38] Laird. Thermoelectric handbook. 2012. Available from: www.Lairdtech.com.